Geophysical Journal International

Advancing Astronomy and Geophysics

doi: 10.1093/gji/ggz269

Geophys. J. Int. (2019) **219**, 290–296
Advance Access publication 2019 June 10
GJI Geomagnetism, Rock Magnetism and Palaeomagnetism

AF demagnetization and ARM acquisition at elevated temperatures in natural titanomagnetite bearing rocks

Michael W. R. Volk[®], ^{1,2} Michael Eitel³ and Mike Jackson^{®2}

- Department of Earth and Planetary Sciences, Harvard University, 20 Oxford Street, Cambridge, MA 02138, USA. E-mail: michael_volk@fas.harvard.edu
- ²Department of Earth Sciences, Institute for Rock Magnetism, University of Minnesota, 116 Church St SE, Minneapolis, MN 55455, USA

Accepted 2019 June 6. Received 2019 April 21; in original form 2019 May 31

SUMMARY

Understanding the temporal changes of the Earth's magnetic field intensity is one of the main goals of modern palaeomagnetism. For most palaeointensity methods to yield reliable results, the magnetic minerals must obey a set of rules. One of these rules is the additivity of partial thermal (TRM) or anhysteretic remanent magnetizations (ARM). Additivity was previously shown for partial TRM in single-domain particles and more generally for ARMs. Additivity between these two low-field remanences, however, has not been investigated, yet. This paper presents a series of rock magnetic experiments on natural low Ti titanomagnetites (Curie temperature between 534 °C and 561 °C) examining the effects of high temperatures on alternating field (AF) demagnetization and acquisition of an ARM. One of our sample sets comes from a borehole drilled through the impact melt sheet of the Manicouagan crater (Canada), the other from the Rocche Rosse lava flow on the island of Lipari (Italy). Hysteresis parameters indicate the magnetic carriers in the pseudo-single-domain range showing no evidence for oxidation. Thermal demagnetization at 300 °C and 500 °C before AF demagnetization shifts the coercivity spectra towards higher fields. AF demagnetization experiments at 500 °C show a significant (by a factor between 1.4 and >7.6) reduction in median destructive field and a shift towards lower coercivities. A linear relationship was found between the peak magnetic field required to demagnetize a fraction of a full TRM of a sample at a specific temperature and the one necessary to demagnetize the same fraction at room temperature after heating to that temperature. The comparison of full ARM and partial TRM at successively higher temperatures with a hybrid hTARM reveals that combined additivity between the two kinds of remanences is fulfilled. These results open the possibility to demagnetize highly coercive minerals, such as hematite and goethite, which is often not achievable at elevated temperatures. Furthermore, the additivity of TRM and ARM remanences may be used to develop novel hybrid TRM/ARM palaeointensity methods for samples, where heating is problematic (e.g. in meteorites).

Key words: Magnetic properties; Rock and mineral magnetism; Remagnetization.

1 INTRODUCTION

Thellier-type palaeointensities are a robust method to estimate the strength of the magnetic field of ancient times. The method has a solid theoretical foundation in Néel theory (Néel 1949). Thellier (1938) has introduced three laws for thermoremanent magnetization in single domain (SD) particles, which need to be fulfilled in order for the result to be valid:

(1) reciprocity: a partial thermal remanent magnetization (pTRM) imparted in a certain temperature interval can be demagnetized by null field thermal cycling through the same temperature interval;

- (2) independence: pTRMs of two non-overlapping temperature intervals do not influence each other;
- (3) additivity: the sum of the pTRMs of two non-overlapping temperature intervals equals the pTRM acquired over the full temperature interval.

These laws have been tested for different minerals and particle sizes (e.g. Levi 1979; Shcherbakova *et al.* 2000; Riisager & Riisager 2001; Shcherbakov & Shcherbakova 2001; Yu & Tauxe 2005). Analogously, reciprocity, additivity and independence of partial anhysteretic remanent magnetizations (pARM) were also tested (Yu *et al.* 2002a,b, 2003). While the law of additivity of pARMs holds for all classes of material (Patton & Fitch 1962), multidomain (MD) grains violate the laws of reciprocity and independence.

³Department of Earth and Environmental Sciences, Ludwig Maximilians University, Theresienstr. 41/IV, 80333 Munich, Germany

The nature of anhysteretic remanent magnetization (ARM) as well as the influence of various parameters on ARM intensity has been subject of numerous studies. Sugiura (1979) found a dependence of the ratios between ARM, TRM and saturation isothermal remanent magnetization on the magnetite concentration within a sample potentially leading to errors of a factor \approx 6 when using the pseudo-Thellier method (e.g. see Tauxe et al. 1995)—although not designed for that-for absolute palaeointensity investigations on natural samples with typical concentrations of magnetite. An analysis of grain size dependence of ARM was performed and compared to MD theory (Stacey 1963) by Gillingham & Stacey (1971). Egli & Lowrie (2002) performed a detailed theoretical study of ARM dependence on parameters such as grain size and alternating field (AF) ramp rate. For magnetite grains up to 60 nm in diameter they found a dependence of ARM intensity on the grain size ($\propto d^2$), temperature $(T^{-2/3})$ and a weak dependence on the ramping rate of the AF.

However, to our knowledge, the combined additivity of TRM and ARMs has not been studied, yet. In this paper, we present a series of experiments imparting pTRMs (pTRM(T)) by in field heating and cooling of the samples to seven temperature steps, T_n , and imparting also ARMs at the respective temperatures, while the heating—cooling process was performed in zero field (ARM(T)). These results are then compared to a combined TRM and ARM obtained by thermal cycling of the samples to the desired temperatures in a laboratory field and imparting an ARM at the target temperature (hTARM(T)).

Furthermore, we show the AF demagnetization behaviour of a full TRM after thermal demagnetization to certain temperature steps, $T_{\rm n}$, and compare it to AF demagnetization performed while samples are held at elevated temperature.

2 SAMPLE DESCRIPTION

Samples 525, 1125 and 1524 are natural samples from the Manicouagan impact crater (Québec, Canada). They are part of core M0608, described in Spray et~al.~(2010), drilled during a commercial mineral exploration program; the sample number represents the core depth in meters. This core was drilled through $\approx 1.5~\rm km$ of clast-free and clast-laden impact melt. The rock magnetic properties of these samples were studied in Eitel et~al.~(2016). The only magnetic remanence carriers are Ti-poor titanomagnetites (Curie temperatures between 550 and 561 °C), with increasing magnetite concentration towards the bottom; in the samples used here, (titano-)hematite is absent.

The second set of samples was collected from the Rocche Rosse (Italy) obsidian flow. These obsidian samples are known for their high thermal stability (Leonhardt *et al.* 2006; Volk & Gilder 2016). The dominating magnetic mineral is low-Ti titanomagnetite with an average Curie temperature of 538 ± 4 °C (Volk & Gilder 2016). No other magnetic mineral phases are present.

3 RESULTS

3.1 Rock-magnetic properties

Hysteresis loops and backfield curves were measured with a LakeShore MicroMag 3900 vibrating sample magnetometer. The hysteresis loops of the samples from the Manicouagan drill core (Fig. 1a; Table 1) are all well saturated by $500 \, \text{mT}$. Saturation magnetizations range from $0.4 \text{ to } 1.3 \, \text{Am}^2 \, \text{kg}^{-1}$, with the highest values

at the bottom of the melt sheet. This effect that is confirmed by susceptibility data (Eitel *et al.* 2016) is interpreted to be caused by a higher titanomagnetite concentration in the lower part of the impact melt due to gravitational differentiation. In these samples, one could expect the magnetic carriers of the upper part to be smaller and thus more SD. On the other hand, the samples from the lower part would be larger due to the longer cooling times and behave more MD. In fact, the remanence ratios ($M_{\rm rs}/M_{\rm s}$) of the three samples are comparable. All samples plot within the pseudo SD (PSD) range (Fig. 1c); just the $M_{\rm rs}/M_{\rm s}$ of the intermediate sample is lower than that of the others.

The samples from Rocche Rosse (Fig. 1b) show a saturation magnetization around 2×10^{-2} Am² kg⁻¹, one to two orders of magnitude less than the Manicouagan samples. Detailed rock magnetic experiments were described in (Leonhardt *et al.* 2006; Volk & Gilder 2016) and showed magnetic carriers in the PSD range. All obsidian samples show similar hysteresis behaviour and parameters, as can be seen in the Day (Day *et al.* 1977; Dunlop 2002) plot in Fig. 1(c). In general, increasing the temperature shifts the magnetic properties of both the Manicouagan and the obsidian samples towards a more MD-like behaviour.

3.2 AF demagnetization

For stepwise AF demagnetization and ARM acquisition, a custommade oven was built using a Pythagoras tube with the heating wires wound around back and forth in a double helix arrangement to avoid magnetic fields generated by the AC heating current. For the temperature isolation of the coil, the oven is surrounded by Promasil, a porous ceramics material of low thermal conductivity; cylindrical plugs close the front and the backside of the oven. The oven was inserted into a shielded 2G AF coil. Three glass tubes assure a gap between the oven and the coil to allow air circulation driven by a fan. The residual field inside the coil was measured with a threecomponent fluxgate magnetometer and is in the order of 10 nT. Prior to each AF demagnetization experiment, a full TRM was imparted to the samples in the direction of the core axis by cooling from 600 °C with a 50 µT field applied in an ASC Scientific Thermal Demagnetizer, TD48. Measurements of the magnetic moment of the samples were performed at room temperature using a JR6 spinner magnetometer. All experiments were performed in the magnetically shielded room at the Ludwig-Maximilians-Universität München.

For each sample, we AF-demagnetized a full TRM under the following conditions: (1) ordinary room temperature demagnetization ($M_0 = M(20 \,^{\circ}\text{C}, \, 20 \,^{\circ}\text{C})$); (2) room temperature AF-demagnetization of a 300 $\,^{\circ}\text{C}$ thermally demagnetized remanence ($M(20 \,^{\circ}\text{C}, \, 300 \,^{\circ}\text{C})$); (3) AF demagnetization while the sample temperature was held at 300 $\,^{\circ}\text{C}$ ($M(300 \,^{\circ}\text{C}, \, 300 \,^{\circ}\text{C})$); (4) room temperature AF-demagnetization after heating to 500 $\,^{\circ}\text{C}$ ($M(20 \,^{\circ}\text{C}, \, 500 \,^{\circ}\text{C})$); (5) AF demagnetization while the sample temperature was held at 500 $\,^{\circ}\text{C}$ ($M(500 \,^{\circ}\text{C}, \, 500 \,^{\circ}\text{C})$). The direction of the AF-demagnetization was along the core axis, which corresponds to the TRM direction. In the following, we denote the remanent magnetization remaining after AF treatment as $M(T_i, T_j)$, with T_i being the sample temperature during AF demagnetization and T_j the maximum temperature of the sample.

Fig. 2 shows the decay of the remanent magnetization for the Manicouagan (a-c) and obsidian (d-f) samples after step-wise AF demagnetization at room temperature (the black line), and when the AF was applied during (the solid lines) as well as after (the dashed

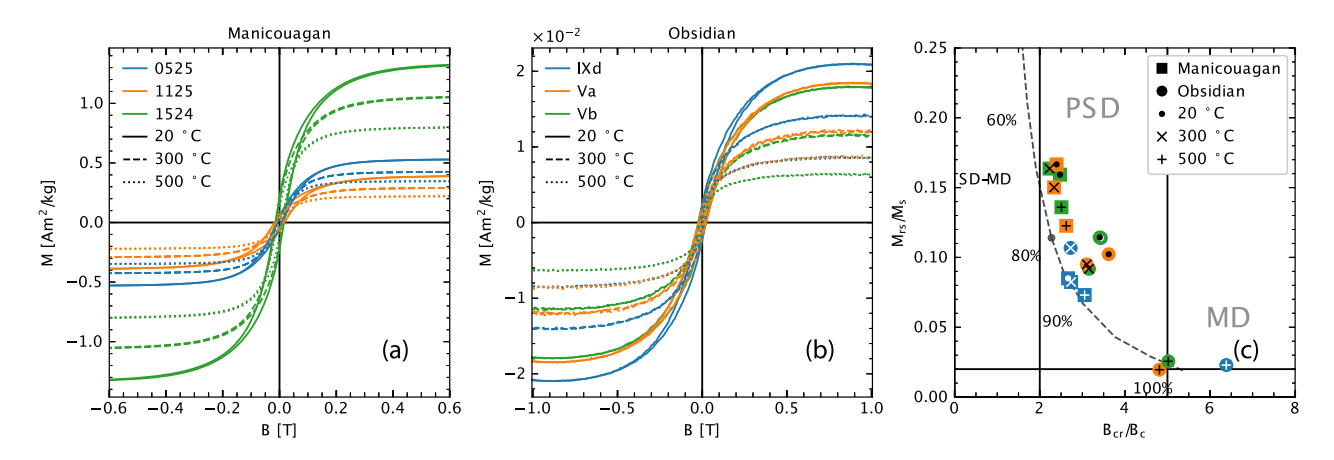


Figure 1. Hysteresis plots of the samples from (a) Manicouagan and (b) Rocche Rosse. (c) Day plot (Day *et al.* 1977) showing all the samples are in pseudo single domain (PSD) state and near or to the right of the mixing line from Dunlop (2002). The square markers show samples from the Manicouagan sample set; the round markers are obsidian samples. The colours correspond to the samples as defined in (a and b).

Table 1. Rock magnetic par	rameters for all	samples determined	from hysteresis lo	oops and backfie	d curves at different
temperatures.					

Sample	<i>T</i> (°C)	$M_{\rm s}$ (mAm ² kg ⁻¹)	$M_{\rm rs}$ (mAm ² kg ⁻¹)	$B_{\rm c}$ (mT)	$B_{\rm cr}$ (mT)	$M_{\rm rs}/M_{\rm s}$	$B_{\rm cr}/B_{\rm c}$
0525	20	530.99	45.16	8.85	23.59	0.09	2.67
0525	300	426.50	35.15	6.93	18.96	0.08	2.74
0525	500	347.61	25.39	5.12	15.63	0.07	3.05
1125	20	391.93	65.31	17.65	42.28	0.17	2.39
1125	300	291.44	43.76	13.00	30.40	0.15	2.34
1125	500	220.48	27.04	8.07	21.15	0.12	2.62
1524	20	1329.99	211.79	15.48	38.33	0.16	2.48
1524	300	1057.25	1173.00	12.96	28.90	0.16	2.23
1524	500	801.91	109.01	8.31	20.84	0.14	2.51
IXd	20	20.92	2.38	21.97	75.44	0.11	3.43
IXd	300	14.06	1.50	13.15	35.84	0.11	2.73
IXd	500	8.54	0.20	1.43	9.10	0.02	6.38
Va	20	18.42	1.88	22.48	81.36	0.10	3.62
Va	300	12.04	1.14	13.52	41.98	0.10	3.10
Va	500	8.61	0.17	1.94	9.35	0.02	4.81
Vb	20	17.90	2.05	22.80	77.70	0.11	3.41
Vb	300	11.48	1.05	13.06	41.20	0.09	3.16
Vb	500	6.34	0.16	1.54	7.71	0.03	5.02

lines) heating to 300 and 500 $^{\circ}$ C. The normalized AF demagnetization curves (Supporting Information Fig. S1 (online) shows nonnormalized values) at room temperature are similar with a slight increase in median destructive field (MDF; Table 2) after removing the magnetic moment of grains with an unblocking temperature lower than 300 and 500 $^{\circ}$ C. When AF demagnetization takes place while the samples are at elevated temperature, however, weaker fields are necessary to demagnetize the samples.

While the decay plots of the obsidian samples are similar (Figs 2d–f), larger differences are expressed in the Manicouagan samples (Figs 2a–c). While samples 525 and 1125 are comparable to each other, the MDF of sample 1524 that possesses a room temperature (T_0) MDF (M_0) of 12.0 mT (about half of the two others) is reduced below 10 mT at 300 °C. This can be attributed to the higher titanomagnetite concentration. The $M(500 \,^{\circ}\text{C}, 500 \,^{\circ}\text{C})$ demagnetization curve of sample 1524 assimilates to those of the two other samples from Manicouagan.

3.3 TRM, ARM and hTARM acquisition

Fig. 3 displays the results for pTRM(T) acquisition, ARM(T) acquisition and hybrid hTARM(T) for samples M1125 and IXd, acquired in a 50 μ T direct field along the sample axis. ARMs were acquired in a 90 mT peak AC-field superimposed with a 50 μ T direct field. The two samples are representative for their respective sample groups and show largely different behaviour. While the Manicouagan samples acquire a pTRM in the first heating step (100 °C), the pTRM of the obsidian samples remains close to zero up to temperatures of 300 °C and increases slowly up to 500 °C. The samples acquire most of their pTRM (>80 per cent) in the narrow temperature window between 500 and 550 °C.

The ARM acquisition of the samples from Manicouagan is relatively temperature independent up to a temperature of $400 \,^{\circ}$ C. At $T > 400 \,^{\circ}$ C ($450 \,^{\circ}$ C for sample 525), the ARM decreases and vanishes (not surprisingly) close to the Curie temperature of the samples

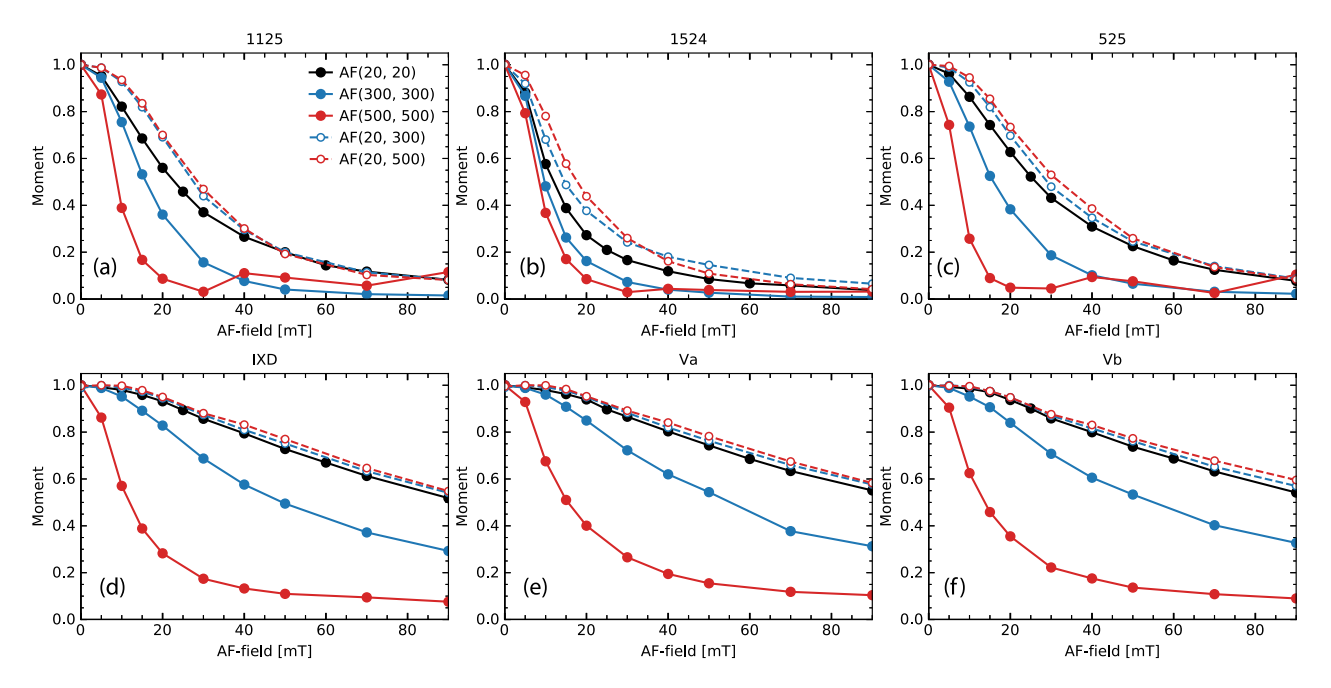


Figure 2. AF demagnetization at elevated temperatures. The solid lines show AF-demagnetization at T_0 , 300 or 500 °C. The dashed lines show AF demagnetization at room temperature after thermally demagnetizing to 300 or 500 °C.

Table 2. MDF and slope for equal demagnetization at different temperatures. MDF(T_0 , T_0) is median destructive field of a TRM with no additional heating, MDF(T_0 , T_n) is MDF of TRM where AF is done at room temperature after thermally demagnetizing to T_n , MDF(T_n , T_n) if MDF where AF is applied at T_n . The maximum AF field was 90 mT. Therefore, values marked with T_n were extrapolated by linear interpolation.

MDF	T_0, T_0	<i>T</i> ₀ , 300 °C	<i>T</i> ₀ , 500 °C	300 °C, 300 °C	500 °C, 500 °C	s(300°C)	s(500 °C)
1125	22.9 mT	27.6 mT	28.7 mT	15.9 mT	8.9 mT	0.59	0.30
1524	12.0 mT	14.7 mT	17.8 mT	9.8 mT	8.4 mT	0.40	0.37
525	26.2 mT	29.1 mT	32.1 mT	15.9 mT	7.5 mT	0.57	0.23
IXd	$93.9\mathrm{mT}^\dagger$	$98.8\mathrm{mT}^\dagger$	$99.8\mathrm{mT}^\dagger$	49.4 mT	11.9 mT	0.51	0.13
Va	$102.3 \mathrm{mT}^{\dagger}$	$108.4\mathrm{mT}^\dagger$	$108.0\mathrm{mT^\dagger}$	55.3 mT	15.5 mT	0.52	0.15
Vb	$99.3 \mathrm{mT}^{\dagger}$	$107.0\mathrm{mT}^\dagger$	$113.2\mathrm{mT}^\dagger$	55.1 mT	13.8 mT	0.52	0.13

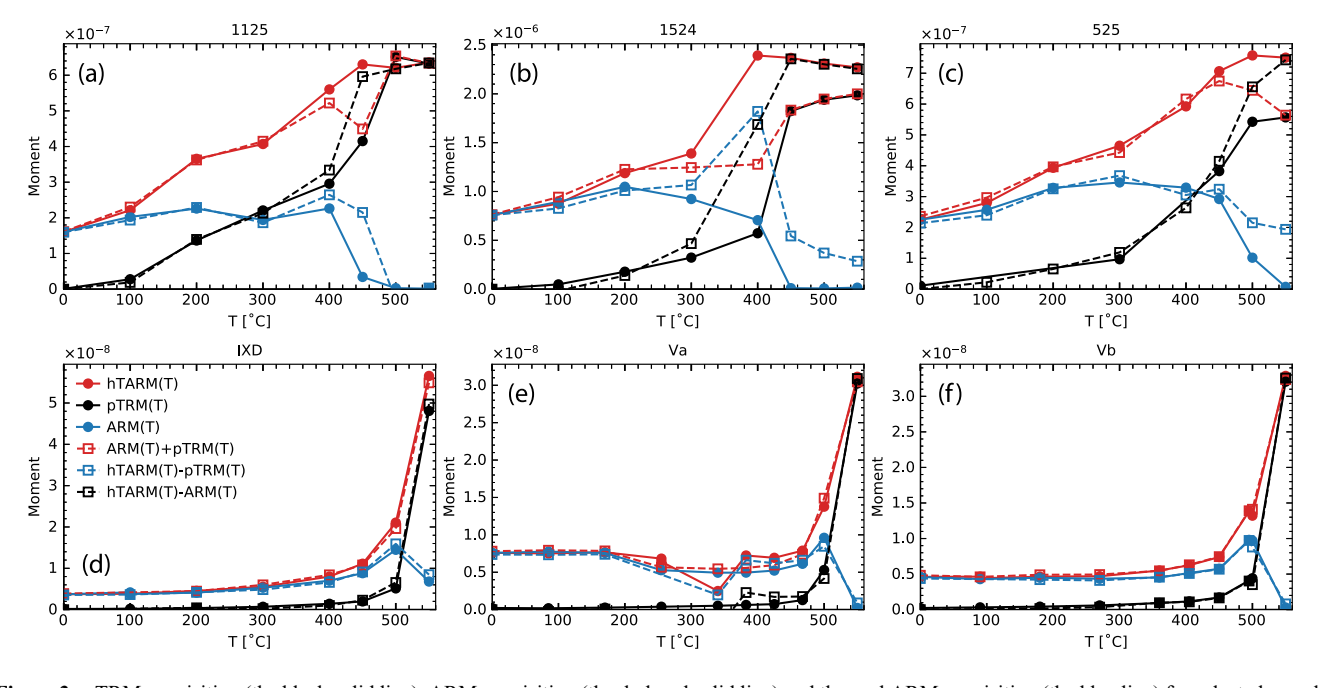


Figure 3. pTRM acquisition (the black solid line), ARM acquisition (the dark red solid line) and thermal ARM acquisition (the blue line) for selected sample. The dashed lines show the additivity of the different acquisition modes.

(550–561 °C). The obsidian samples show similar behaviour. The acquired ARM is constant in the first temperature steps and reaches the maximum value at 500 °C. At higher temperatures the ARM(T) decreases.

4 DISCUSSION

4.1 Coercivity spectra

The room temperature MDFs of the Manicouagan samples are between 12 and 26 mT. When AF demagnetization is performed at 300 °C, they decrease to 10–16 mT; the MDF(500 °C, 500 °C) is about 8 mT for all three samples from Manicouagan. At room temperature, the maximum field (90 mT) of the coil demagnetizes the Obsidian samples (Va, Vb, IXd) only to 54 ± 2 per cent of its initial TRM. Therefore, calculation of the MDF is not possible. Linear interpolation of the data indicates coercivities around 100 mT (marked by † in Table 2). Increasing the temperature lowers the MDF(300 °C, 300 °C) of the obsidians to 49–55 mT and the MDF(500 °C, 500 °C) to 12–16 mT. This demonstrates the temperature dependence of the coercivity of titanomagnetites.

Furthermore, Fig. 2 and Table 2 show that the MDF of the samples is raised by a zero field heating cooling cycle before an AF demagnetization. This effect occurs because the particles with lower coercivities also possess lower unblocking temperatures ($T_{\rm UB}$), and so, the fraction of the magnetically weakest particles has already thermally been demagnetized. As a consequence, the AF demagnetization, which then can take place only on the remaining—harder—particles, becomes less efficient.

Fig. 4 shows the derivative of the decay plots from Fig. 2. Compared to the room temperature AF demagnetization of the manicouagan samples, the loss of magnetization is shifted towards higher demagnetizing fields, when the sample is demagnetized after it was exposed to $T_{\rm n}=300~{\rm ^{\circ}C}$ or $500~{\rm ^{\circ}C}$. The derivatives of the decay curves of the obsidians, however, do not show any differences after the treatment. In the case of AF demagnetizing the sample while kept at $T_{\rm p}$, the coercivity spectrum is shifted and squeezed towards lower fields. While for the Manicouagan samples the maximum measured value of the derivative stays constant at $10 \,\mathrm{mT}$, at T_0 and $T_{\rm n} = 300 \,^{\circ}{\rm C}$ the true maximum seems to lie between 10 and 15 mT, at $T_n = 500$ °C between 5 and 10 mT. As the magnetization is now demagnetized in a smaller AF-interval, the maximum value of the derivative becomes higher. This is also true for the obsidian samples, but here, the maximum of the derivative is shifted from 25 mT at room temperature to 20 mT at 300 °C and to 10 mT at 500 °C. This observation also confirms that in the case of the Manicouagan samples thermal demagnetization at moderate temperatures affects the same grains that were demagnetized in AFs up to 20 mT, and thus, apparently raises the coercivity of the sample.

4.2 Additivity

The dashed red lines in Figs 3(a)–(f) represent the sum of the ARM(T) and pTRM(T) curves. In the case of perfect additivity of ARM and pTRM, these curves fall together with the hybrid hTARM curves. For sample M1125, both curves are in good agreement with each other, with a maximum deviation of 6.8 per cent, disregarding the outlier at 450 °C. Also in the case of the obsidian sample IXd, deviations never exceed 8.3 per cent, and are absent below 500 °C. The differences of pTRM(T) (black) and ARM(T) (blue) from the

hybrid hTARM measurement are shown for comparison with the ARM(T) and pTRM(T) curves, respectively.

The fact that the combined additivity of pTRM and ARM is fulfilled in the samples used in our experiments, can be explained as follows: During the pTRM acquisition, all grains with a blocking temperature below the actual temperature step T_i are magnetized after cooling to room temperature (T_0) . In the case of the ARM acquisition at elevated temperature, only those grains with a coercivity $B_c(T_i > T_0) < 90 \,\mathrm{mT}$ are magnetized and these also have a blocking temperature higher than T_i , as all grains with $T_B < T_i$ stay demagnetized due to cooling to room temperature in zero field. For the hybrid hTARM acquisition, however, in the ARM acquisition step, again, the grains with $B_c(T_i > T_0) < 90 \,\mathrm{mT}$ and $T_B > T_i$ are magnetized, but during in field cooling to room temperature, all grains with $T_{\rm B} < T_{\rm i}$ are magnetized, regardless of their coercivity. Hence, the grains that acquire a pTRM plus the grains that acquire an ARM are exactly those that are magnetized in the hybrid hTARM acquisition step.

4.3 Thermal fluctuations

Thermal fluctuations have been described by Néel (1949) as a hypothetical magnetic field ($B_{\rm th}$), which acts on particles to reduce their coercivity. $B_{\rm th}$ shifts the coercivity spectrum towards lower fields when AF-demagnetization is done at elevated temperatures. Dunlop (1976) and later Jackson *et al.* (2006) developed methods using thermal fluctuation analysis to calculate the magnetic grain size.

As a generalization of the MDF, one can define the field at which any specified percentage of the initial magnetic moment is lost (e.g. B_{10} being the field where 10 per cent of the initial moment is lost). These fields of equivalent demagnetization were calculated using linear interpolation of the AF-demagnetization data. When the values for the thermally demagnetized samples (AF(T_0 , T_n)) are compared to the AF at elevated temperature (AF(T_n , T_n)) a linear relationship is found for all samples (Fig. 5). A similar almost linear relationship can be seen in the data of Dunlop & Bina (1977) when the same analysis is performed.

In samples 525 and 1125 (Figs 5a–c), the $B_n(T_0) - B_n(T_n)$ slopes (s in Table 2) for the experiments at 300 °C are the highest obtained from all analysed samples (e.g. 0.59 for sample 1125). Here, heating has the least influence on coercivity. Further heating to 500 °C reduces the slope to 0.30. If the slopes of sample 1524 are not forced to the origin, the lines at 300 °C and 500 °C are nearly parallel, with the AF demagnetization at 500 °C being 3–5 per cent more efficient than at 300 °C. The slopes of the obsidian samples (Figs 5 d-f) are more homogeneous with slopes between 0.51 and 0.52, which approximately correspond to the Manicouagan samples. However, when AF demagnetization is carried out at 500 °C, the slope of the samples decrease to only 0.13. From this relationship, it would be possible to estimate the room temperature MDF of the obsidian samples by dividing the MDF at temperature by the calculated slope. Overall, an increased effect of temperature on the AF demagnetization can be seen in the case of the obsidians compared to the Manicouagan samples.

All of the samples, however, exhibit a weak, but systematic deviation from linearity (Fig. 5). In the first demagnetizing steps, the $B_{\rm n}(T_0)-B_{\rm n}(T_{\rm n})$ values are below the average slope, increasing above the slope, when 20–50 per cent of the initial magnetization has been lost through AF demagnetization at elevated temperature.

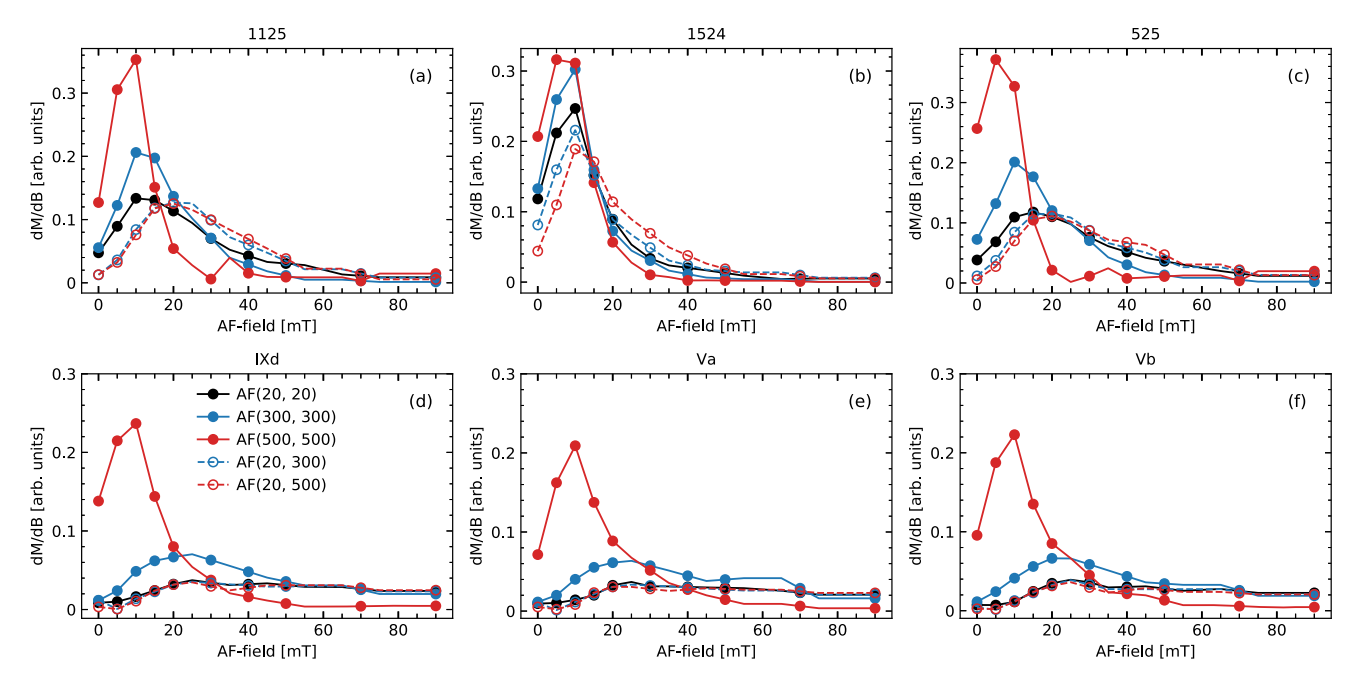


Figure 4. Derivatives of the AF decay plots of representative samples M1125 (a) and IXd (b) at room temperature (black), after thermal treatment (the open symbols) and at temperature (the solid symbols), representing the coercivity spectra of the grains with $T_B > T_i$.

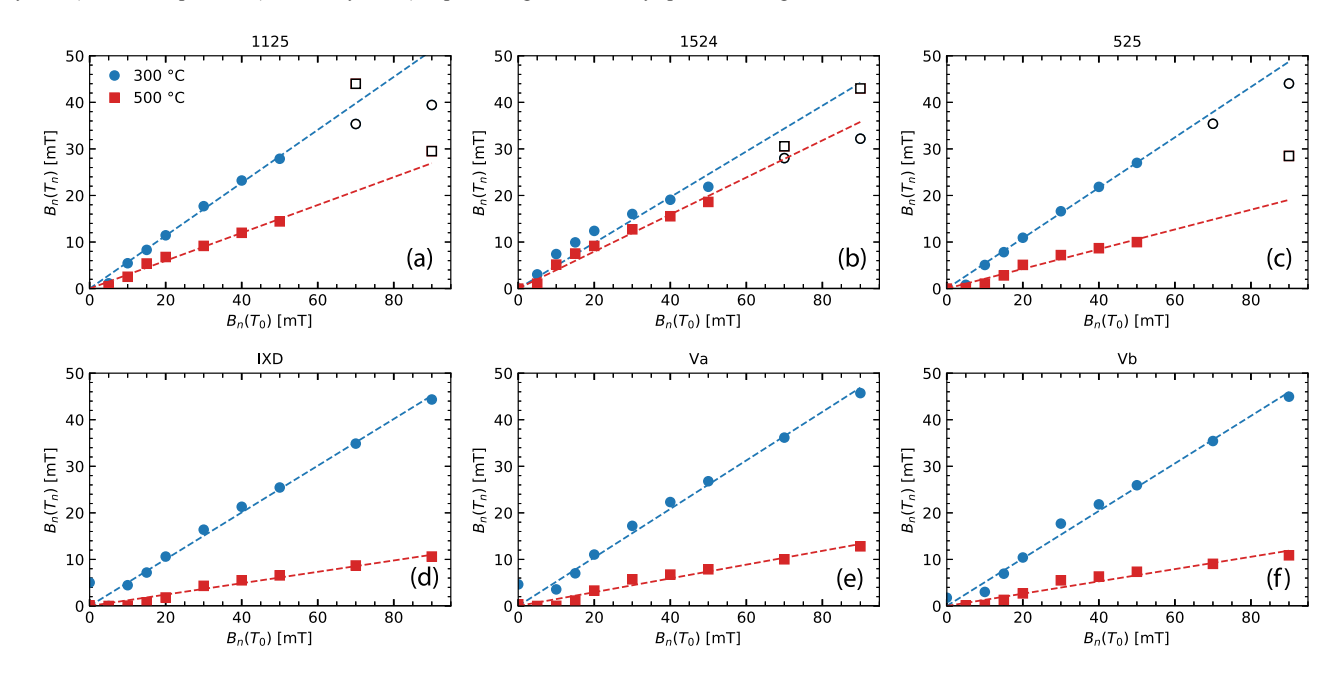


Figure 5. Field of equivalent demagnetization, the field needed to demagnetize the same amount of magnetic moment. The open markers show points that have been excluded in the linear regression line. The slope is proportional to the field needed to demagnetize the same amount of moment at elevated temperatures compared to room temperature.

At the highest demagnetization levels, the $B_n(T_0) - B_n(T_n)$ values again fall below the average trend. Elucidation of the reason for the S-shaped form of the data curve still remains subject of research.

5 CONCLUSIONS

This study has confirmed the reduction of coercivities and a shift of the coercivity spectra with increasing temperature for two sets of rock samples containing natural Ti-poor titanomagnetite of PSD domain state similar to the results on synthetic Ti-free magnetite of Dunlop & Bina (1977). This change in coercivity is expressed in a close to linear relationship between fields of equivalent demagnetization (e.g. MDF) at different temperatures. That opens the possibility to carry out AF demagnetization experiments on magnetically hard samples, when the samples can be heated.

Furthermore, we showed that Thellier's law of additivity, which applies for thermoremanent magnetization in SD particles (Thellier 1938) as well as for ARM (Patton & Fitch 1962; Yu *et al.* 2002a)

is also valid for a combination of both kinds of magnetization. The fact that coercivities are decreasing with increasing temperature and ARM(T) + TRM(T) are additive, could be used to establish a palaeointensity method, for samples that cannot be easily heated (e.g. meteorites).

ACKNOWLEDGEMENTS

Funding for the Project by Deutsche Forschungsgemeinschaft, SPP 1488 (planetary magnetism). We acknowledge John Spray (Planetary and Space Science Centre, University of New Brunswick) for providing the samples from Manicouagan, and Bettina Scheu (LMU München) for providing the samples from Lipari. Part of this work was performed at the Institute for Rock Magnetism (IRM) at the University of Minnesota. The IRM is a US National Multiuser Facility supported through the Instrumentation and Facilities program of the National Science Foundation, Earth Sciences Division, and by funding from the University of Minnesota. This is IRM publication (#1817).

REFERENCES

- Day, R., Fuller, M. & Schmidt, V., 1977. Hysteresis properties of titanomagnetites: grain-size and compositional dependence, *Phys. Earth* planet. Inter., 13(4), 260–267.
- Dunlop, D.J., 1976. Thermal fluctuation analysis: a new technique in rock magnetism, J. geophys. Res., 81(20), 3511–3517.
- Dunlop, D.J., 2002. Theory and application of the day plot (M_{rs}/M_s) versus H_{cr}/H_c) 1. Theoretical curves and tests using titanomagnetite data, J. geophys. Res., **107**(B3).
- Dunlop, D.J. & Bina, M.-M., 1977. The coercive force spectrum of magnetite at high temperatures: evidence for thermal activation below the blocking temperature, *Geophys. J. Int.*, 51(1), 121–147.
- Egli , R. & Lowrie, W., 2002. Anhysteretic remanent magnetization of fine magnetic particles, J. geophys. Res., 107(B10), EPM 2-1-EPM 2-21.
- Eitel, M., Gilder, S.A., Spray, J., Thompson, L. & Pohl, J., 2016. A paleomagnetic and rock magnetic study of the manicouagan impact structure: implications for crater formation and geodynamo effects, J. geophys. Res., 121(2), 436–454.
- Gillingham, D.E.W. & Stacey, F.D., 1971. Anhysteretic remanent magnetization (ARM) in magnetite grains, *Pure appl. Geophys.*, 91(1), 160–165.
- Jackson, M.J., Carter-Stiglitz, B., Egli, R. & Solheid, P.A., 2006. Characterizing the superparamagnetic grain distribution f(V, Hk) by thermal fluctuation tomography, *J. geophys. Res.*, 111(B12).

- Leonhardt, R., Matzka, J., Nichols, A. & Dingwell, D., 2006. Cooling rate correction of paleointensity determination for volcanic glasses by relaxation geospeedometry, *Earth planet. Sci. Lett.*, 243(1-2), 282–292.
- Levi, S., 1979. The additivity of partial thermal remanent magnetization in magnetite, Geophys. J. Int., 59(1), 205–218.
- Néel, L., 1949. Théorie du trainage magnétique des ferromagnétiques en grains fins avec applications aux terres cuites, Ann. Géophys., 5(2), 99– 136.
- Patton , B.J. & Fitch, J.L., 1962. Anhysteretic remanent magnetization in small steady fields, J. geophys. Res., 67(1), 307–311.
- Riisager, P. & Riisager, J., 2001. Detecting multidomain magnetic grains in Thellier palaeointensity experiments, *Phys. Earth planet. Inter.*, 125(1-4), 111–117
- Shcherbakov, V.P. & Shcherbakova, V.V., 2001. On the suitability of the Thellier method of palaeointensity determinations on pseudo-single-domain and multidomain grains, *Geophys. J. Int.*, **146**(1), 20–30.
- Shcherbakova, V.V., Shcherbakov, V.P. & Heider, F., 2000. Properties of partial thermoremanent magnetization in pseudosingle domain and multidomain magnetite grains, *J. geophys. Res.*, 105(B1), 767–781.
- Spray, J.G., Thompson, L.M., Biren, M.B. & O'Connell-Cooper, C., 2010.
 The Manicouagan impact structure as a terrestrial analogue site for lunar and martian planetary science, *Planet. Space Sci.*, 58(4), 538–551.
- Stacey, F., 1963. The physical theory of rock magnetism, *Adv. Phys.*, **12**(45), 45–133.
- Sugiura, N., 1979. ARM, TRM and magnetic interactions: concentration dependence, Earth planet. Sci. Lett., 42(3), 451–455.
- Tauxe, L., Pick, T. & Kok, Y.S., 1995. Relative paleointensity in sediments: a pseudo-Thellier approach, *Geophys. Res. Lett.*, **22**(21), 2885–2888.
- Thellier, E., 1938. Sur l'aimantation des terres cuites et ses applications géophysiques, PhD thesis, Université de Paris.
- Volk, M.W.R. & Gilder, S.A., 2016. Effect of static pressure on absolute paleointensity recording with implications for meteorites, *J. geophys. Res.*, 121(8), 5596–5610.
- Yu, Y. & Tauxe, L., 2005. Testing the IZZI protocol of geomagnetic field intensity determination, Geochem. Geophys. Geosyst., 6(5).
- Yu, Y., Dunlop, D.J. & Özdemir, Ö., 2002a. Partial anhysteretic remanent magnetization in magnetite 1. additivity, *J. geophys. Res.*, 107(B10), EPM 7–1-EPM 7-9.
- Yu, Y., Dunlop, D.J. & Özdemir, Ö., 2002b. Partial anhysteretic remanent magnetization in magnetite 2. reciprocity, *J. geophys. Res.*, 107(B10), EPM 8-1-EPM 8-9.
- Yu, Y., Dunlop, D.J. & Özdemir, Ö., 2003. Are ARM and TRM analogs? Thellier analysis of ARM and pseudo-thellier analysis of TRM, *Earth planet. Sci. Lett.*, 205(3-4), 325–336.